Materials and Design 162 (2019) 130–142

Contents lists available at ScienceDirect

Materials and Design

journal homepage: www.elsevier.com/locate/matdes

Compressive behaviour of 3D printed thermoplastic polyurethane honeycombs with graded densities

Simon R.G. Bates*, Ian R. Farrow, Richard S. Trask

Bristol Composites Institute (ACCIS), Department of Aerospace Engineering, University of Bristol, Queen's Building, University Walk, Bristol, BS8 1TR, UK

HIGHLIGHTS

- Hyperplastic honeycombs with 4 density grading methodologies were produced via fused filament fabrication 3D-printing.
- All thermoplastic polyurethane honeycombs were subjected to quasi-static, cyclic and high strain-rate impact analysis.
- By density grading, energy absorbing and damping profiles were significantly modified from the uniform density equivalent.
- Samples absorbed specific impact energies of up to 270 mJ/cm^3 at strain-rates of up to 51 s^{-1} before recovering elastically.
- Lower peak loads were transferred for graded samples for the most severe impact cases.

GRAPHICAL ABSTRACT

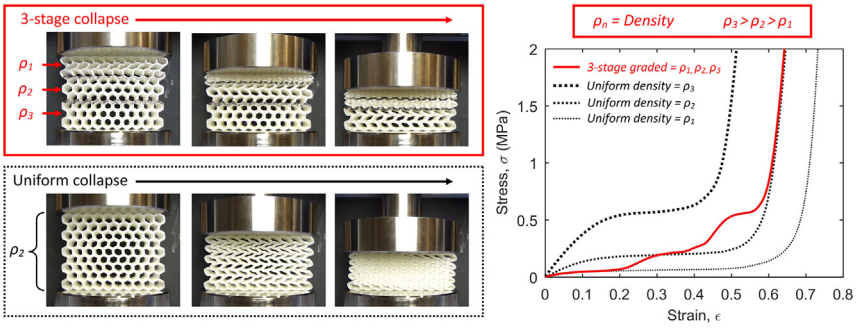

ARTICLE INFO

Article history:
Received 17 September 2018
Received in revised form 5 November 2018
Accepted 7 November 2018
Available online 14 November 2018

Keywords:
Additive manufacturing
Cellular structures
Functional grading
Thermoplastic polyurethane

ABSTRACT

Fused filament fabrication of thermoplastic polyurethanes (TPUs) offers a capability to manufacture tailorable, flexible honeycomb structures which can be optimised for energy absorbing applications. This work explores the effect of a range of grading methodologies on the energy absorbing and damping behaviour of flexible TPU honeycomb structures. By applying density grading, the energy absorbing and damping profiles are significantly modified from the uniform density equivalent. A 3D-printing procedure was developed which allowed the manufacture of high-quality structures, which underwent cyclic loading to densification without failure. Graded honeycomb architectures had an average relative density of 0.375 ± 0.05. After quasi-static testing, arrays were subjected to sinusoidal compression over a range of amplitudes at 0.5 Hz. By grading the structural density in different ways, mechanical damping was modified. Cyclic compressive testing also showed how strain-softening of the TPU parent material could lead to reduced damping over the course of 50 cycles. Samples were subjected to impact loading at strain-rates of up to 51 s^{-1} and specific impact energies of up to 270 mJ/cm^3. Lower peak loads were transferred for graded samples for the most severe impact cases. This behaviour reveals the potential of density grading of TPU structures to provide superior impact protection in extreme environmental conditions.

* Corresponding author.
E-mail address: s.r.g.bates@bristol.ac.uk (S.R. Bates).

https://doi.org/10.1016/j.matdes.2018.11.019

1. Introduction

Cellular materials and structures are utilised in a large number of energy absorbing applications ranging from cheap packaging [1] to space craft landing gear [2]. This is due to their high specific strength and excellent energy absorbing properties. Such structures can be manufactured from polymers, metals, ceramics, glasses and composite materials [3]. Traditionally, cellular materials are formed in bulk processes such as foaming, or in the case of honeycombs, via adhering, welding, brazing, extrusion or thermally fusing sheets of material [4,5]. These manufacturing techniques produce cellular structures with either isotropic or orthotropic material properties. However, it has been shown that by instead producing cellular structures with non-uniform architectures and properties, their mechanical and energy absorbing performance can be greatly enhanced [6-14].

In particular, density grading has been shown to be an effective method for tailoring the energy absorbing properties of cellular structures. A numerical study by Ajdari et al. [15] showed that by grading the density of a honeycomb in 5 discrete regions, the deformation-mode and energy absorption characteristics could be significantly modified from the equivalent uniform density structure. In dynamic crushing simulations, it was shown that density grading could significantly improve energy absorption of a honeycomb, when the high density face was impacted, up to compressive strains of 50%. In another numerical study, Cui et al. [16] found that by applying functional grading methodologies to foam, the energy absorption properties were superior when compared to the equivalent uniform foams, at low impact energies. The authors noted this to be greatest when a convex density gradient was applied.

The potential for improved energy absorption via density grading has also been shown in practical studies. In work by Gupta [17], layers of syntactic foam with varying volume fractions of glass microballoons were stacked and adhered to form functionally graded syntactic foams. These foams absorbed between 300% and 500% more energy than uniform syntactic foams when compressed at quasi-static loading rates of 1 mm/min. Hangai et al. [18] discussed the advantages of forming functionally graded aluminium foams for crash structures. They observed that the sequential deformation of a functionally graded foam could be controlled at the desired location at the desired stress, for superior crash protection. By creating aluminium foams via a friction stirring process, they showed that there was potential to achieve the desired staggered collapse under quasi-static compression. Brothers and Dunand [19] created similar foams by casting a replica of a polymeric graded precursor.

Unfortunately, the manufacturing techniques used to form functionally graded foams are complex, expensive and offer a poor level of control of local architecture. This is not the case for cellular structures with larger unit cells such as lattices and honeycombs. These structures can be manufactured via established 3D printing technology, and the local cellular architectures, precisely controlled. In a study by Maskery et al. [20], cellular lattices with graded densities were manufactured from nylon 12 via selective laser sintering (SLS) 3D printing. In quasi-static testing, graded density lattices with a relative density of 0.19 absorbed over twice the energy of the uniform density equivalent. This marked increase in energy absorption was attributed to densification (full collapse of the lattice struts) occurring at a higher strain and the generation of a highly non-linear energy absorption profile. Although showing the potential for density grading for tailoring energy absorption, these and other similar studies into density grading [21,12] have focused on single compression cases and do so because the materials used deform plastically and fail by brittle fracture under load.

Materials which undergo large-strain elastic recovery may however be utilised in fused filament fabrication (FFF) 3D printing. Zhang et al. demonstrated that honeycombs 3D printed from polycaprolactone had the potential to recover by 80% after a single compression to densification [22]. Despite the apparent recovery, significant plastic deformation was observed in the material at compressive strains over 20% and recovery was reduced after subsequent cycles.Thermoplastic polyurethanes (TPUs) are block copolymers known to have excellent impact properties and abrasion resistance [23] and as such have great potential as materials for building energy absorbing structures. In a recent study, Ge et al. utilised a TPU parent material to produced a flexible Kelvin foam structure on a commercially available FFF 3D printer [24]. Samples of the Kelvin foam structure were cycled 100 times to 87% compressive strain demonstrating their viability as rubber-like energy absorbers, rather than single-use cushion materials. A previous study by the authors also demonstrated that the same TPU material could be used to form resilient energy absorbing honeycombs [25]. Uniform honeycombs with a range of densities were produced and were shown to recover elastically after being subject to 5 compressive cycles to densification. Importantly, these honeycombs demonstrated energy absorbing efficiencies comparable to that of polyurethane foams.

The behaviours of recoverable, elastic honeycomb structures which also include an element of density grading are, however, yet to be explored. Such structures could have far reaching applications in the field of personal protection against extreme environments. It is the aim of this work to extend our previous study into the energy absorbing behaviour of uniform density flexible TPU honeycombs [25] to explore how functional density grading may affect the energy absorbing response of such structures. It is hypothesised that, by including a range of densities within an individual honeycomb structure, it may be possible to absorb a range of impact energies efficiently. This behaviour is not seen in uniform density TPU honeycombs [25] or for any uniform density cellular structure [3]; these structures instead have a single impact energy which they are optimised to absorb. Achieving this would aid the design of high performance energy absorbing structures for practical environments where a large range of impacts must be efficiently absorbed. In this work, this possibility is explored by assessing honeycombs with basic structural grading, via quasi-static and dynamic compressive testing. In order to create elastic, recoverable honeycombs, FFF 3D printing of TPUs was utilised.

2. Materials and manufacture

2.1. TPU material properties

All honeycombs were manufactured from NinjaFlex® TPU which was produced by Fenner Drives Inc. The density of the TPU was measured as $\rho_s = 1235\,\mathrm{kg/m^3}$. Tensile tests of the 3D printed NinjaFlex TPU specimens were carried out in accordance with ASTMD412 [26] and these tests showed stress-strain behaviour that was linear at low strains, becoming less stiff and highly non-linear at strains, $\epsilon > 0.03$. Dogbone samples were produced for these tests via FFF 3D printing with the primary print direction at 0° to the extension direction. The low strain modulus of the NinjaFlex was $E = 21.2 \pm 1.1\,\mathrm{N/mm^2}$ and the ultimate tensile strength of the TPU was $\sigma_{UTS} = 28.1 \pm 0.4\,\mathrm{N/mm^2}$. For comparison with other 3D printing techniques, this is 28× the tensile strength of flexible TangoPlus material used in Polyjet 3D printing [27].

2.2. 3D printing graded cellular structures

All specimens were produced via FFF 3D printing using an Ultimaker Original desktop 3D printer [28]. This machine was based upon the one used to produce uniform density TPU honeycombs in previous work by the authors [25], where high quality samples

were produced with no visible voidage. For this study, the Ulimaker Original was adapted to increase soft material 3D printing performance by installing a Flex3Drive [29] filament extruder. In previous work [25], the Ultimaker ran using the standard "Bowden extruder" set-up whereby the 3 mm TPU filament was driven by a stepper motor through a 400 mm long PTFE Bowden tube before it entered the printer nozzle. As a result, print head speeds had to be limited to 20 mm/s to avoid excessive filament compression and buckling which could lead to manufacturing defects. The Flex3Drive reduced the compression length of the filament to less than 40 mm as the filament drive gear was mounted directly above the printer nozzle. This set-up allowed twice the print head speeds previously achievable, whilst still maintaining high quality samples.

An example structure exhibiting 3 stages of density grading is shown as a design schematic and as a final part in panels a and b in Fig. 1 respectively. When printing uniform density honeycombs, each cell wall was constructed from two adjoining lines (nozzle passes) such that the internal bond-line in which air may be trapped was smeared [25]. This procedure could not be used for printing the graded structures since the wall thicknesses vary within the structures. Instead, the nozzle diameter used to print each structure was matched to approximately twice the smallest wall thickness. This resulted in the printing of "infill" in the cells with larger wall thickness. This can be seen in Fig. 1c which shows a visualisation of the filament print path for a section of the 3-stage graded specimen. The disadvantage of using an infill is that it greatly increases the number of bond lines within the structure and therefore increases the likelihood of manufacturing imperfections. To address this, the outer "shell" lines were printed first and then the infill printed second with higher extrusion values than those recommended in Cura slicing software [31]. The material flow was increased to the maximum value where the shell would contain the infill, ensuring the bond lines were smeared and the cell wall thickness not adversely affected.

Four specimens with graded densities through their structures were produced along with three specimens with constant density for reference. All graded cellular arrays were designed with wall length, $l = 4.65$ mm and an average cell wall thickness, $t_a = 1.6$ mm. The wall thicknesses were graded through the structures from $t = 0.8$ mm to $t = 2.4$ mm as illustrated for the 3-stage graded

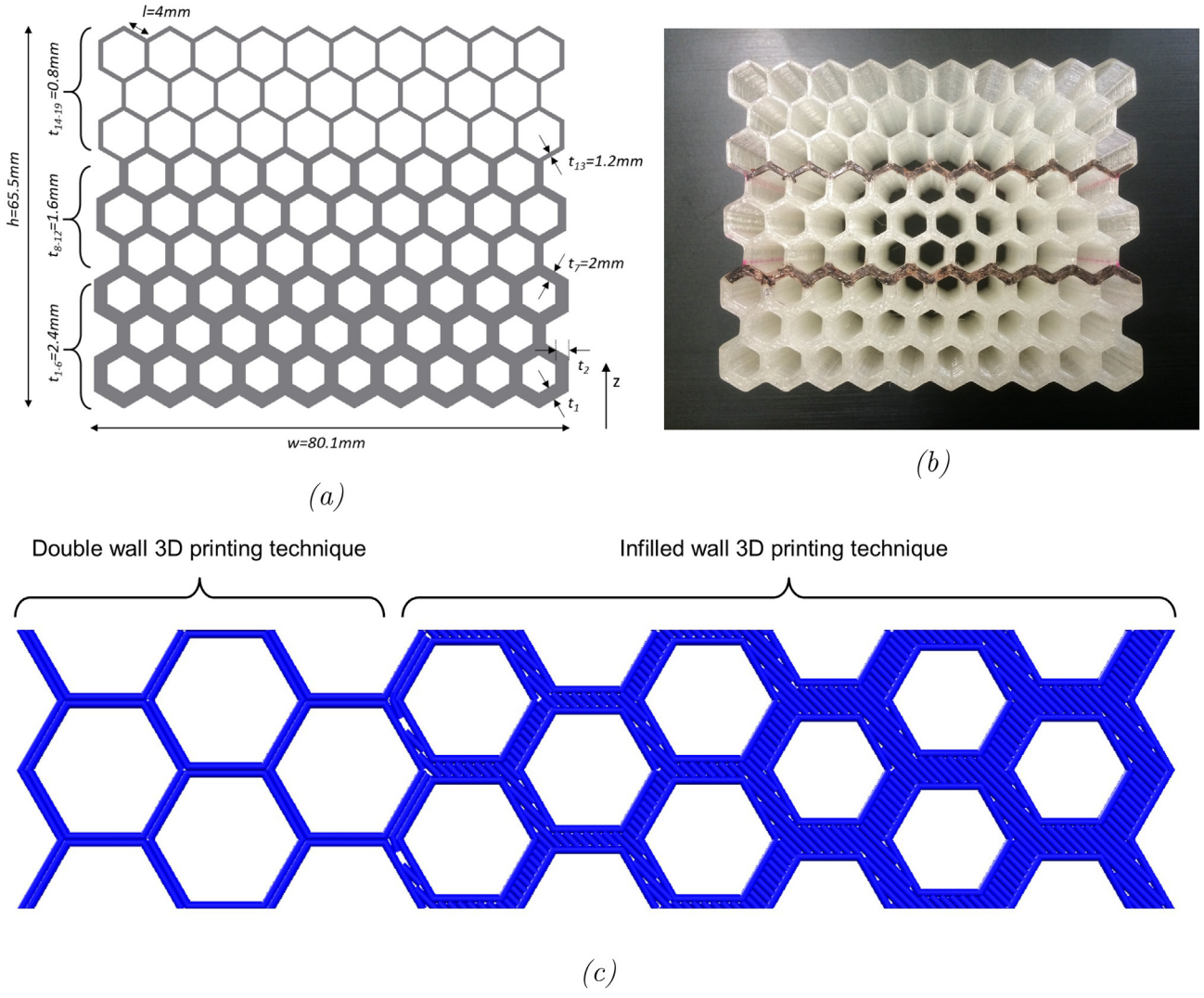

Fig. 1. (a) Design details of the 3-stage graded hexagonal structure. Cell walls are numbered n = 1–19 from the base of the structure and corresponding thickness values, t_n are indicated; (b) the test specimen produced by FFF 3D printing from TPU; the walls of intermediate thickness are indicated in black; (c) the filament print path through the 3-stage graded hexagonal structure visualised in Repetier Host software [30].

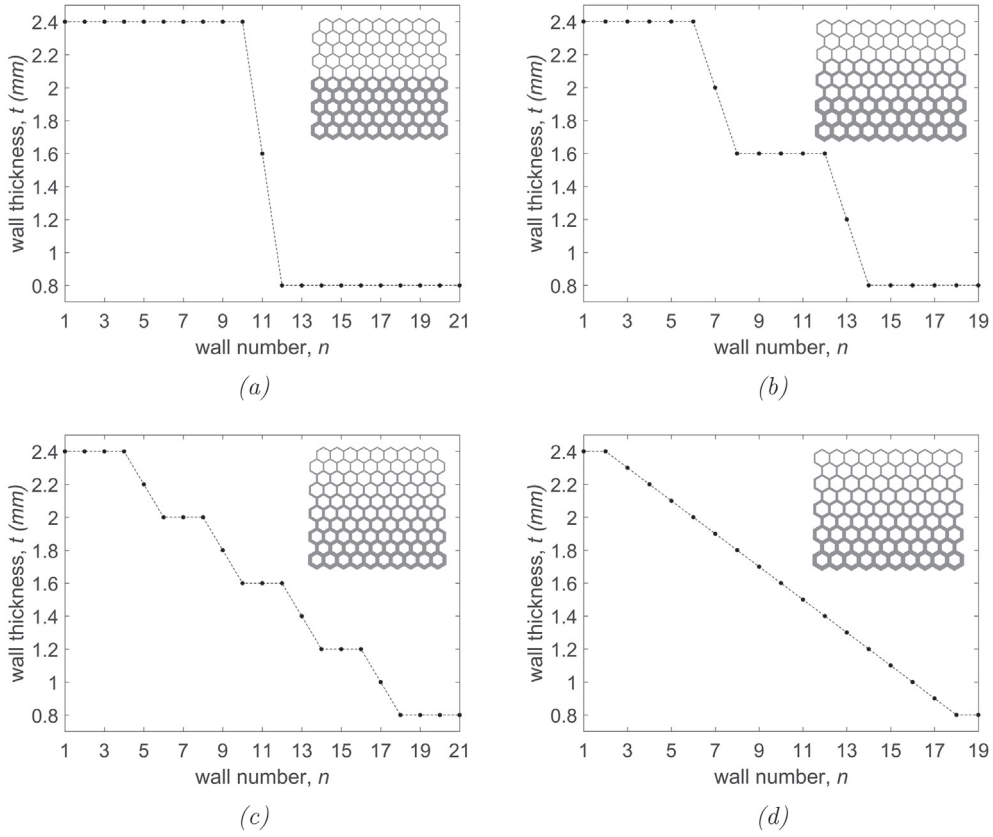

Fig. 2. Graphical representation of the wall thickness of (a) 2-stage; (b) 3-stage; (c) 5-stage and (d) continuously stage graded specimens. The wall numbering system corresponds to that in Fig. 1a. Renderings of the corresponding hexagonal structures are inset.

structure in Fig. 1a. Panels a–d in Fig. 2 detail the wall thickness of the continuously, 5-stage, 3-stage and 2-stage graded structures respectively. The low, medium and high density reference samples were designed with wall length, $l = 4.65$ mm and thicknesses of $t = 0.8$, 1.6 and 2.4 mm respectively. The theoretical relative density for a hexagonal array with constant wall length and thickness is equal to $\rho^*_{RD} = (2/\sqrt{3})(t/l)$ [3] and for a graded structure design, it holds that the average relative density, $\rho^*_{aRD} = (2/\sqrt{3})(t_a/l)$ where t_a is the average wall thickness. The measured relative densities, ρ_{aRD} of the final 3D printed specimens were calculated such that $\rho_a/\rho_s = \rho_{aRD}$, where ρ_a = specimen mass/the cuboidal volume which it occupies. The wall thicknesses of the produced parts were within ±0.2 mm of the design values. Table 1 gives details of the dimensions, relative density and number of rows of hexagonal cells in the manufactured specimens.

3. Experimental methods

3.1. Quasi-static compression

Flat-plate, quasi-static compression tests of the hexagonal arrays were carried out using a Shimadzu AGS-X static test machine with a ±10 kN load cell at room temperature. All samples were compressed in the −z direction as indicated in Fig. 1a under displacement control. A constant strain rate, $\dot{\epsilon} = 0.03\,s^{-1}$ was maintained up to a maximum load of 5 kN to ensure complete densification. The samples were then unloaded at the same rate and this process was repeated for 5 cycles. The data presented in this work was captured on the 5th compressive cycle, at a minimum sampling frequency of 10 Hz. The deformation behaviour of all the specimens was recorded using a high definition camera. Nominal strains, ϵ of the samples were

Table 1
Dimensional properties of the graded honeycombs measured after manufacture.

Specimen details	Number of walls	Height, h (mm)	Width, w (mm)	Depth, d (mm)	Relative density, ρ_{RD}
High density	19	66.2	81.7	29.8	0.50
Medium density	19	65.5	81.1	29.7	0.37
Low density	19	64.5	80.7	29.6	0.26
Continuous grading	19	65.4	81.1	29.7	0.38
5-stage grading	21	72.5	81.2	29.7	0.37
3-stage grading	19	65.5	81.1	29.6	0.38
2-stage grading	21	72.0	81.7	29.8	0.37

recorded by measuring the change in deflection at the interface of the samples with the steel plates. The nominal stress, σ was calculated by dividing the recorded force by the initial projected top surface area of each sample. All data was post-processed using MATLAB software.

3.2. Sinusoidal compression

Samples were subsequently compressed sinusoidally at 0.5 Hz between flat plates using an Instron 1341 hydraulic test machine with a ±27 kN load cell, to analyse their damping behaviour. All arrays were compressed to a strain of 5% and then cycled for 50 cycles to a designated peak strain. Each sample underwent 5 tests which corresponded to the 5 peak strains of 10%, 20%, 30%, 40% and 50%. Force-displacement data was gathered at a minimum sampling frequency of 100 Hz and converted to stress and strain in the same manner as for the quasi-static testing. The areas within the stress-strain loops which resulted from cycling were calculated in order to find the energy dissipated per cycle.

3.3. Impact testing

All samples were finally subjected to flat plate impact testing using an Instron Dynatup 9250HV drop tower; the boundary conditions of the drop testing mimicked those of the quasi-static and cyclic testing. Each specimen was subjected to a range of impacts of increasing specific impact energy from 36 to 270 mJ/cm^3 by increasing the height from which the 7.03 kg mass was dropped. All tests were recorded using a Photron FASTCAMS SA-Z high speed camera at a minimum of 2000 frames per second so the collapse behaviour of the structures could be observed. The force-displacement data was converted to stress and strain in the same manner as for the quasi-static and sinusoidal compression test and compared to the uniform density samples.

4. Results and discussion

4.1. Quasi-static testing

The stress-strain behaviour of the 2-stage, 3-stage, 5-stage and continuously graded structures are shown in panels a–d in Fig. 3 respectively. The behaviour of the graded structures is shown in the continuous black lines and the data for the uniform density reference samples is shown by dotted lines. Panels a–c in Fig. 4 show the corresponding cellular collapse behaviour uniform density ($\rho_{RD} = 0.37$), 3-stage graded and continuously graded specimens respectively.

In Fig. 3, clear plateau regions can be observed for the 2-stage and the 3-stage graded honeycombs indicating a staggered compressive collapse associated with the regions of increasing density within the structure. The clearly defined plateaus are an indication that, for the 2-stage and 3-stage graded specimens, each density region underwent linear deformation, collapse and densification before the succeeding, higher density layer underwent significant deformation.

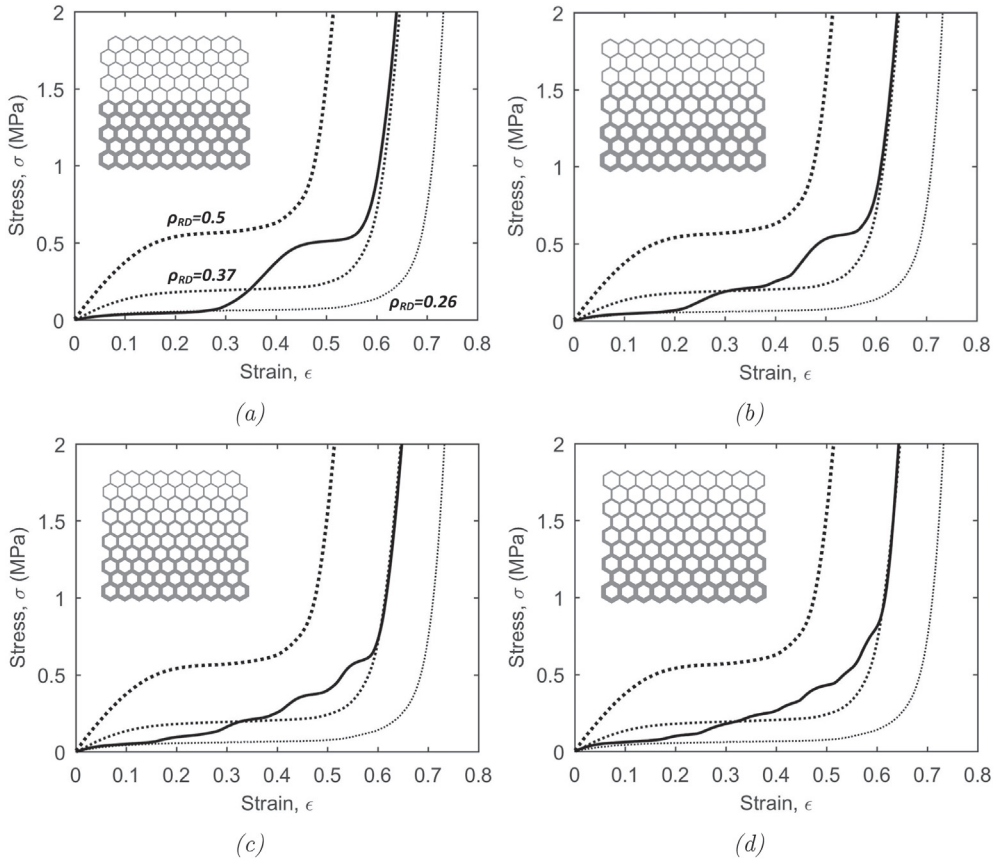

Fig. 3. Stress-strain behaviour of the (a) 2-stage; (b) 3-stage; (c) 5-stage and (d) continuously graded structures (solid lines). The stress-strain behaviours for the low, medium and high density structures are included for reference (dotted lines) with the relative densities, ρ_{RD} shown next to the respective curves in (a).

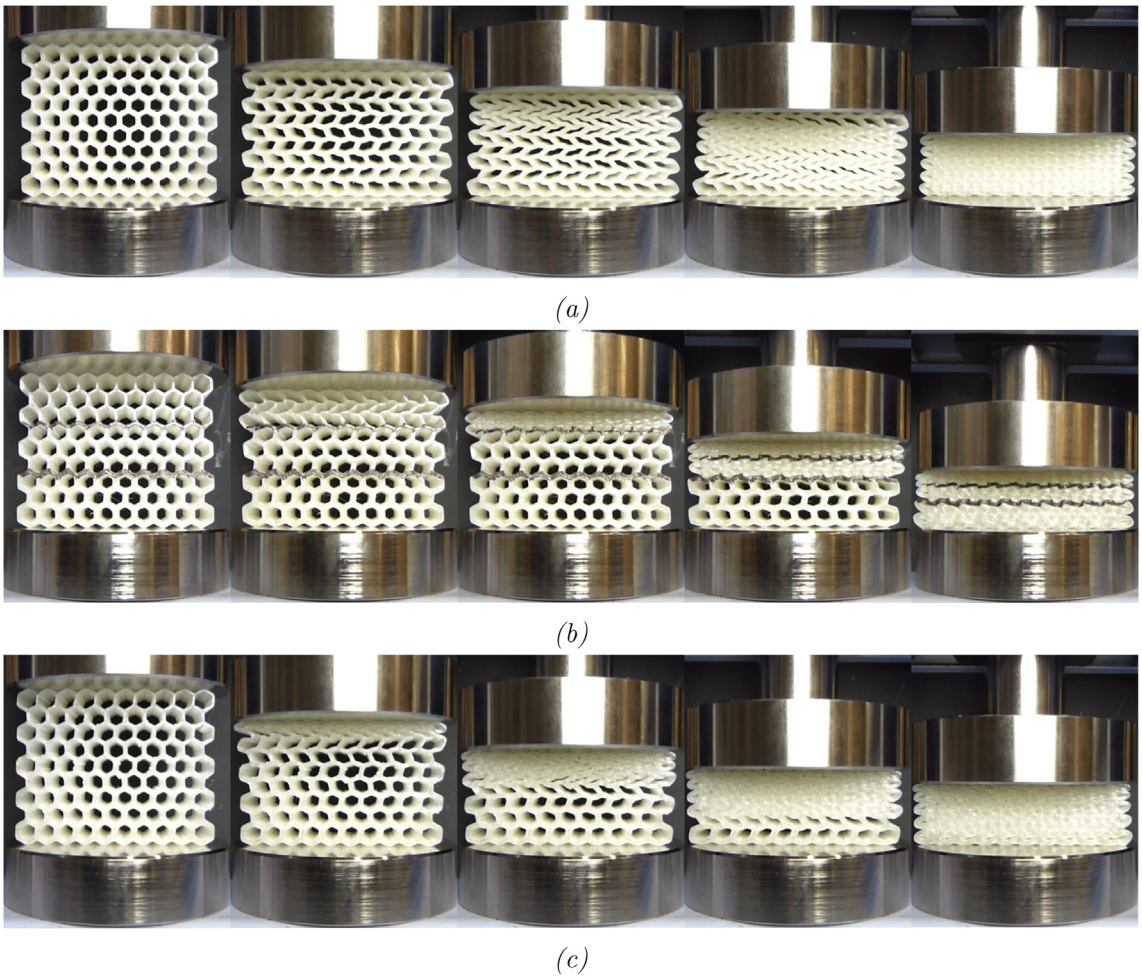

Fig. 4. The cellular collapse behaviour during quasi-static compression of the (a) medium density uniform array ($\rho_{RD} = 0.37$); (b) 3-stage graded array and (c) the continuously graded array.

This staggered cellular collapse can be seen for the 3-stage graded honeycomb in Fig. 4b where the three distinct density regions (black marker lines show the interface between density regions) clearly collapse independently. This behaviour differs significantly from the uniform density sample ($\rho_{RD} = 0.37$) shown in Fig. 4a whose walls buckle uniformly throughout the structure.

Between the plateau regions of the stress-strain profiles, clear transition regions can be distinguished for the 2-stage and 3-stage graded specimens. The 5-stage and continuously graded structures have less well defined plateau regions and transition regions. This occurs due to the onset of significant deformation of the successive, higher density layers before the previous region has undergone full densification. This behaviour can be seen in Fig. 4c which shows the compression of the continuously graded array. Although collapse progresses in a layer-wise manner through the structure, significant deformation of higher density rows can be observed before the full densification of the previous lower density row. For all the graded honeycombs, the length of the individual plateaus decreases as the densities of the layers being compressed increases. Importantly, the strain to densification of the final layers of the graded structure is always greater than that of the equivalent uniform density structure. Maskery et al. [20] observed that graded density lattices densify at higher strains than the uniform density equivalent structures and concluded that this contributed to their superior energy absorbing properties. Despite densifying at higher strains than the uniform equivalent sample, the behaviour upon complete densification for all of the graded structures tracks the same stress-strain path as the equivalent uniform density sample.

In this study, energy absorption diagrams have been used to asses the behaviour of the graded density honeycomb structures. This methodology was first presented by Maiti, Gibson and Ashby for the characterisation of the energy absorbing behaviour of cellular structures [3]. These diagrams are formed from the compressive stress-strain data from a group of similar cellular structures with a range of densities or topologies, by integrating the area under the curves to calculate the specific energy absorbed in J/cm^3 and plotting against stress. These diagrams allow the appropriate energy absorbing structure to be chosen to protect against an impact with a known specific energy, by selecting the structure which would transfer the lowest stress. A detailed explanation of how these diagrams may be used for the assessment of uniform density TPU honeycombs is given in [25].

Panels a–d in Fig. 5 show energy absorption diagrams for the 2-stage, 3-stage, 5-stage and continuously graded structures respectively. The data for the graded structures is shown in solid black and the uniform density reference samples are shown by the dotted lines.

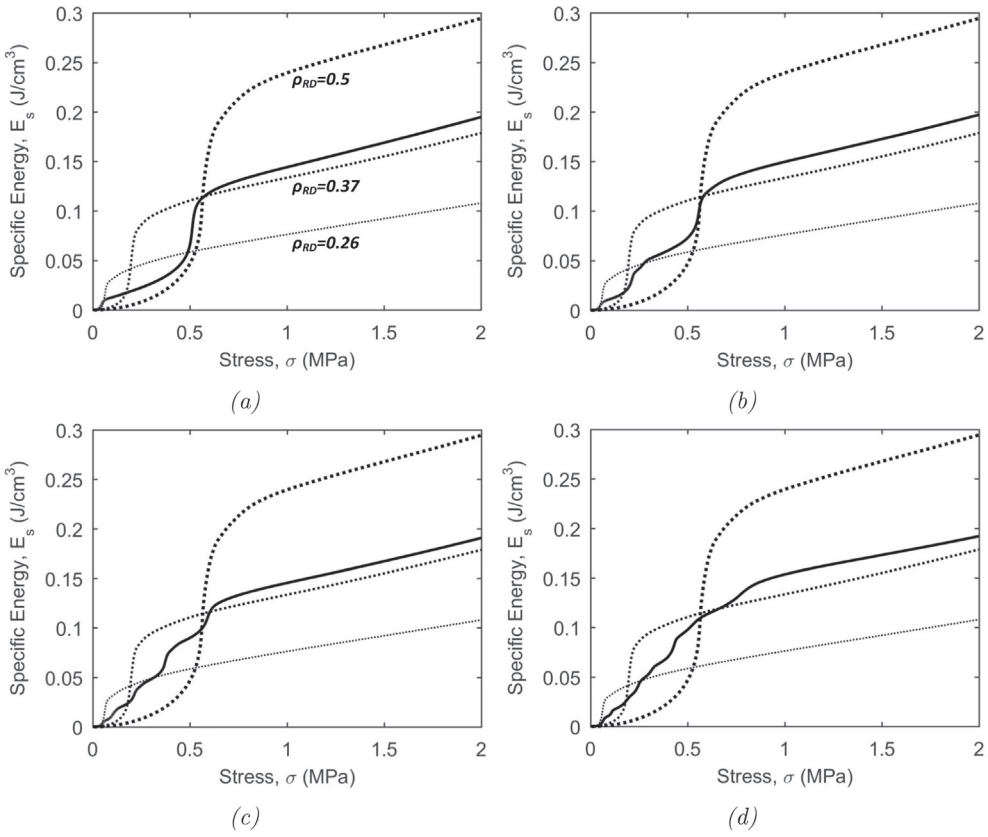

Fig. 5. Energy absorption diagrams for (a) 2-stage; (b) 3-stage; (c) 5-stage and (d) continuously graded structures (solid lines). The energy absorption behaviours for the low, medium and high density structures are included for reference (dotted lines) with the relative densities, ρ_{RD} shown next to the respective curves in (a).

Consistent with behaviour seen previously [25] the uniform density honeycomb profiles have a single shoulder point. This shoulder corresponds to a point of optimum energy absorption efficiency [32] and is defined in this work as the point of the onset of densification. The energy absorption profiles of the graded structures reflect the fluctuations observed in the stress-strain profiles (see Fig. 3) such that the energy-stress curves of the graded structures have a series of shoulder points rather than a singular shoulder. The number of shoulder points is equal to the number of graded layers through the structure. The shoulder points are well defined for the 2-stage, 3-stage and 5-stage graded structures and could be connected with a single straight line with equal gradient for all honeycombs.

The total amount of energy absorbed by the graded structures was on average $11 \pm 3\%$ higher than that of the equivalent uniform structure at a compressive stress of 1 MPa. The believed cause for this higher total energy absorption, despite the samples having the same average density, is the non-linear relationship between the structural density and energy absorption and the higher strain to densification.

An efficient energy absorbing structure absorbs large amounts of energy whilst transferring a low stress. Therefore a more efficient structure would reside further to the left of the energy absorption diagram. The curve of the continuously graded structure resides to the left of the uniform ($\rho_{RD} = 0.37$) structure at energies below 26 mJ/cm^3 and above 119 mJ/cm^3. This means that this graded structure is more efficient at absorbing energy at high or low energy compressions. There is however a wide range of intermediate energies that the uniform structure is better suited to absorb. Similar behaviour is seen for all the graded structures. The poorest performing graded structure in the intermediate range is the 2-stage structure due to its lack of any intermediate density layers. The wide range of densities in the continuous structure mean that it is the most efficient of the graded structures in the intermediate energy range. It should be noted that another equivalent form that the energy absorption diagram can take is the efficiency diagram [32]. For reference, efficiency diagrams which correspond to Fig. 5a–d are included in Supplementary information S1.

4.2. Sinusoidal cyclic compression

Panels a–e in Fig. 6 show the cyclic compressive stress-strain behaviour of uniform, 2-stage, 3-stage, 5-stage and continuously graded structures respectively. Each plot shows the cyclic compressive behaviour from the 50th cycle of 5 separate tests; the samples were pre-strained to 5% and then cycled to either 10%, 20%, 30%, 40% or 50% compressive strain in each of the tests. The loading and unloading cycle in each case occurs in the clockwise direction and the loading portion of each curve takes on a similar profile to that of the quasi-static tests.

Due to the presence of layers of high relative density, at large compressive strains, the stresses transferred by the graded structures far exceed that of the uniform structure. Due to the viscoelastic nature of the parent material, the unloading portion of the cyclic compression curve tracks lower stress values than the loading portion of the same cycle. Further, the TPU parent material also undergoes a strain-softening response which is dependent on the magnitude of the compressive strain to which it has been subjected [33]. As a result, the samples appear softer when repeatedly cycled

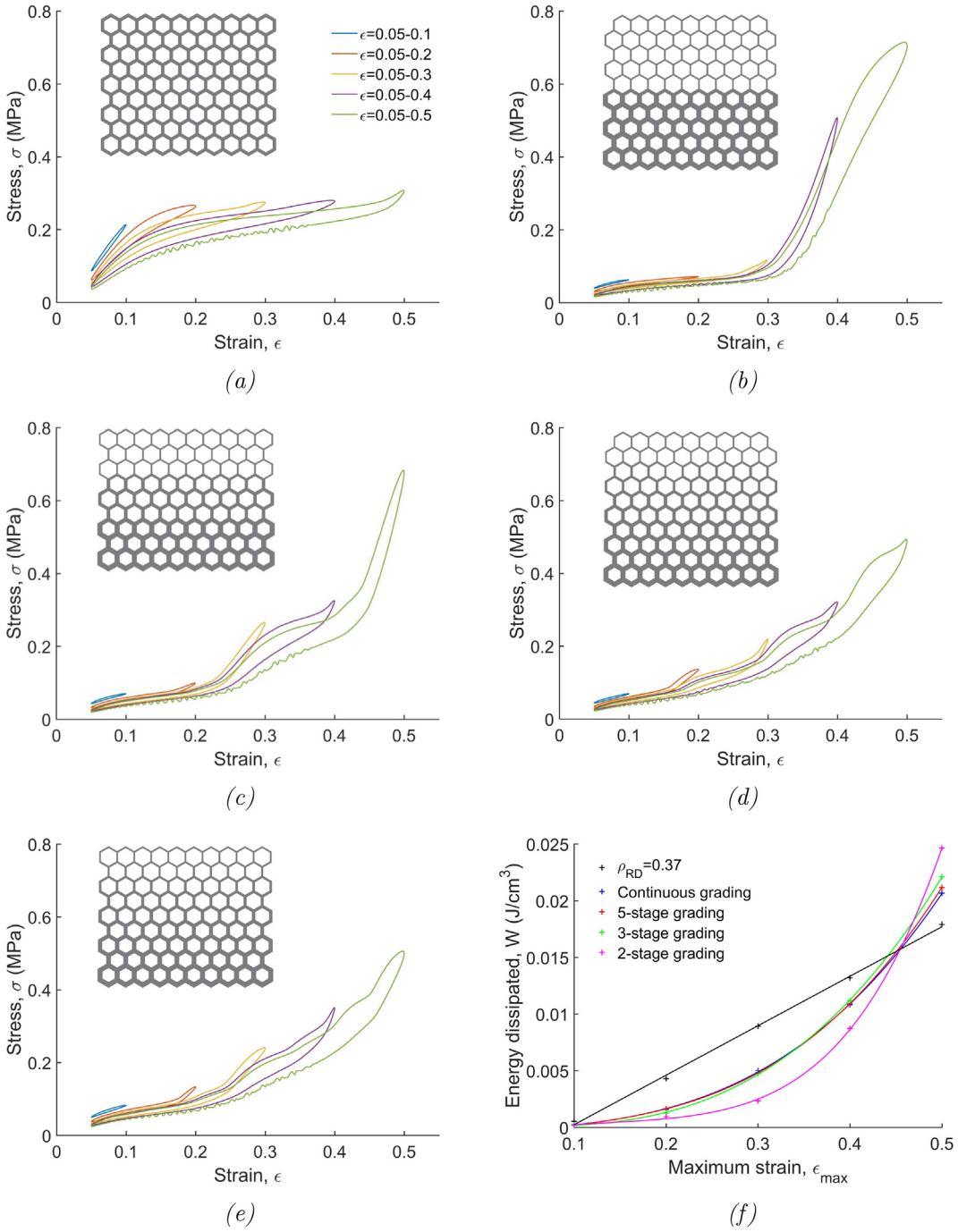

Fig. 6. Cyclic compressive stress-strain response of (a) uniform density, (b) 2-stage graded, (c) 3-stage graded, (d) 5-stage graded and (e) continuously graded structures compressed between 5% and 10, 20, 30, 40 and 50% compressive strain. (f) The specific energy dissipated in each compressive cycle for each structure in each of the 5 tests with unique maximum strains, ϵ_{max}.

to a higher maximum strain. The damping of a structure is proportional to the area within the closed hysteresis loop which is formed during cycling [34]; for a stress-strain plot this area gives the specific energy dissipated in a single cycle in J/cm^3.

Fig. 6 shows the specific energy dissipated in each compressive cycle for each structure in each of the 5 tests with unique maximum strains, ϵ_{max}. The energy dissipated by the uniform density structure increases in a linear manner with increasing maximum strain. The energy dissipated by the structures with an element of density grading increased in a non-linear manner with increasing maximum strain. This non-linear increase can be attributed to the fact that, at low strains, only the lower density part of the structures are being compressed and therefore less material is deforming. The damping capacity of all the structures is lower than that of the uniform density structure in all but the case where they are compressed to $\epsilon = 0.5$. At high strains, the graded structures provide greater damping as well as absorbing more energy. By varying the type of density grading, it can be seen here that the peak stress, energy

Table 2
Experimental variables for impact tests of graded density honeycombs with 9 rows. Experimental variables detailed are as follows: Drop height, H_d; impact velocity, v; impact strain rate, $\dot{\epsilon}_{int}$; impact energy, E_T; specific impact energy, E_S; and average recorded impact energy, E_S^*.

Experiment	H_d (m)	v (m/s)	$\dot{\epsilon}_{int}$ (s^{-1})	E_T (J)	E_S (mJ/cm^3)	E_S^* (mJ/cm^3)
1	0.069	1.16	17.8	4.8	30	36 ± 1.5
2	0.126	1.58	24.1	8.7	55	64 ± 0.6
3	0.184	1.90	29.0	12.7	80	91 ± 0.6
4	0.241	2.18	33.3	16.7	105	117 ± 0.2
5	0.299	2.42	37.0	20.7	130	143 ± 0.3
6	0.357	2.65	40.4	24.6	155	167 ± 1.4
7	0.414	2.85	43.6	28.6	181	192 ± 0.6
8	0.472	3.04	46.5	32.6	205	220 ± 0.8
9	0.530	3.22	49.2	36.6	230	245 ± 0.7
10	0.587	3.40	51.8	40.5	255	270 ± 0.2

absorption and damping behaviour may be modified. There is potential to explore how density grading may be modified beyond these simple strategies, in order to tune these parameters to suit different energy absorbing applications.

4.3. Impact behaviour

After being subjected to cyclic compressive loading, all honeycomb architectures were then subjected to drop-tower impact tests. It was observed from the quasi-static behaviour of the graded density honeycombs that the graded structures absorbed low and high impact energies efficiently, whilst the uniform density structure absorbed intermediate energies more efficiently. In order to observe whether this behaviour would translate to higher strain rate impacts, each specimen was subjected to a series of impacts of increasing energy and the force-deflection data captured in each test. The 3-stage graded, continuously graded and uniform density honeycombs all contained 9 cell rows whereas the 5-stage graded and 2-stage graded honeycombs contained 10 rows as detailed in Fig. 2a–d. Because of this, the 5-stage graded and 2-stage graded honeycombs were slightly taller and therefore had a larger volume. In order to make sure the impacts imparted to each honeycomb were equivalent, each honeycomb was subjected to the same 10 impacts with respect to the specific impact energy, E_S. Since E_S equals the total impact energy, E_T divided by the specimen volume, v, the specimens with a larger volume were subjected to slightly higher impact energies. The impact energy of each test was controlled by varying the drop height and maintaining the mass of the impactor, which was measured as 7.03 kg using the drop tower load cell.

The force-displacement results from the drop tower generated from each test were integrated up until the point of maximum compressive displacement. This gave the recorded energy of impact which was in turn divided by the volume of the specimen to get the recorded specific energy of impact, E_S^*. In theory, the 'designed', E_S and 'recorded', E_S^* energy of impact should be equal. In this instance, the recorded impact energies were on average 12 mJ/cm^3 higher than the designed, indicating a calibration error in the drop weight measurement. The recorded energy of impact, E_S^* is a more accurate measure of the impact energy imparted and therefore will be quoted as the impact energy when discussing the results. Both E_S and E_S^* for each of the tests are given in Tables 2 and 3 along with the other experimental variables for honeycomb architectures with 9 rows and 10 rows respectively. Each honeycomb was held in place on an immovable base plate with masking tape and subjected to increasing impact energies at an interval of 2 min between impacts. The specimens were free to expand laterally under compression but remained on the base plate during compression and rebound. The boundary conditions therefore mimicked those used in quasi-static and cyclic compressive testing.

Panels a–d in Fig. 7 show the high speed camera images of the uniform density sample, whilst in panels e–h in Fig. 7 the behaviour of the 3-stage graded sample and in panels i–l in Fig. 7 the behaviour of the continuously graded sample subjected to the largest impact energy of 270 mJ/cm^3. The initial strain rate at impact was $\dot{\epsilon}_{int} = 51\ s^{-1}$ in all cases. The deformation behaviour of the samples differ very little from the quasi-static compression tests, despite the increased strain rate. There is a slight indication in Fig. 7b and c that the cells closest to the impactor begin collapsing sooner than those nearest the immovable plate however if this is the case, the effect is minor. Such behaviour is not seen in rigid honeycombs until impact velocities are higher than 30 m/s [35]. Fig. 7d, h and l shows the maximum deflection of the uniform density, 3-stage

Table 3
Experimental variables for impact tests of graded density honeycombs with 10 rows. Experimental variables detailed are as follows: Drop height, H_d; impact velocity, v; impact strain rate, $\dot{\epsilon}_{int}$; impact energy, E_T; specific impact energy, E_S; and average recorded impact energy, E_S^*.

Experiment	H_d (m)	v (m/s)	$\dot{\epsilon}_{int}$ (s^{-1})	E_T (J)	E_S (mJ/cm^3)	E_S^* (mJ/cm^3)
1	0.076	1.22	16.9	5.3	30	36 ± 1.5
2	0.140	1.66	22.9	9.6	55	64 ± 0.6
3	0.203	2.00	27.7	14.0	80	91 ± 0.6
4	0.267	2.29	31.7	18.4	105	117 ± 0.2
5	0.330	2.55	35.2	22.8	130	143 ± 0.3
6	0.394	2.78	38.5	27.2	155	167 ± 1.4
7	0.458	3.00	41.5	31.6	181	192 ± 0.6
8	0.521	3.20	44.3	35.9	205	220 ± 0.8
9	0.585	3.39	46.9	40.3	230	245 ± 0.7
10	0.648	3.57	49.4	44.7	255	270 ± 0.2

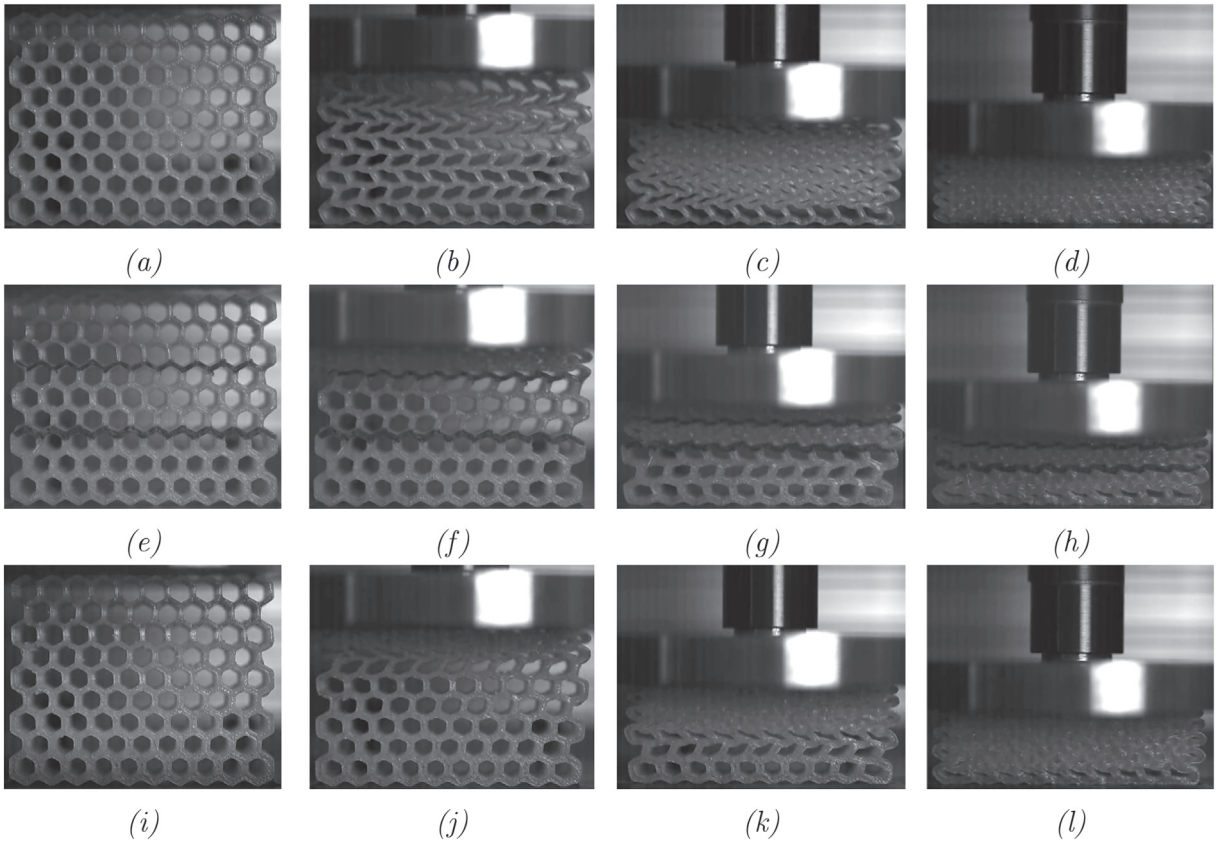

Fig. 7. Deformation behaviour of uniform density (a–d), 3-stage graded (e–h) and continuously graded (i–l) honeycombs subjected to a specific impact energy of 270 mJ/cm^3. From left to right the images show deformation at compressive strains $\epsilon = 0$, 0.25, 0.5 and ϵ_{max}. $\epsilon_{max} = 0.68$, 0.64 and 0.64 for the uniform, 3-stage graded and continuously graded honeycombs respectively.

graded and continuously graded honeycombs. Although all three honeycombs were subjected to the same impact energy, the uniform density sample can be seen to completely densify whereas the graded samples did not. This would imply that the graded samples more efficiently absorb this large impact energy then the uniform sample; this can be confirmed by examining the corresponding force -time plots in Fig. 8.

Panels a–c in Fig. 8 show the force-time plots for all honeycombs subjected to impacts with specific energies of 36 mJ/cm^3, 143 mJ/cm^3 and 270 mJ/cm^3 respectively. In each diagram, the peak force which was transferred by the uniform density honeycomb is included for reference. For the impact of 36 mJ/cm^3 the uniform density sample transfers a slightly higher load than all the graded density structures. This occurs because all the graded density structures have absorbed the impact energy using the cellular rows with a density lower than that of the uniform density sample. For intermediate impact energy of 143 mJ/cm^3, the peak load transferred by the uniform density honeycomb is significantly lower than that of the graded honeycombs. In order to absorb this energy, in the graded structures, the cellular rows with higher densities than that of the uniform density structure had to be compressed and therefore higher loads were transferred. The uniform density structure is acting efficiently at this energy as characterised by the long flat plateau. For the highest impact energy of 270 mJ/cm^3, the uniform density structure transfers a higher load than that of the graded structures as it has undergone significant densification; this is characterised by the steep increase in force/time gradient at 12ms into the impact.

Although all the graded structures had begun to compress their most dense cellular row, significant densification was not induced by this impact; this reflects the behaviour seen in Fig. 7d, h and l. The behaviour seen in these force-time plots is consistent with the prediction from the quasi-static, i.e.that the graded structures were more efficient at absorbing low and high impact energies, whereas the uniform density structure absorbs intermediate impact energy betters.

For comparison, panels a–d in Fig. 9 show the high strain rate ($\dot{\epsilon}_{int} = 51\,s^{-1}$) and low strain rate ($\dot{\epsilon} = 0.03\,s^{-1}$) stress-strain behaviour of the 2-stage, 3-stage, 5-stage and continuously graded structures respectively. The stress-strain curves for the high strain rate conditions were formed from the force-deflection data gathered from the 270 mJ/cm^3 impact tests. The graded structures transfer higher stresses when compressed at the higher strain rate, with the effect being more pronounced when the higher density regions are compressed. Further, the stress plateaus which were flat in the case of the quasi-static testing, undulate for the high strain rate tests, exhibiting short regions of negative stiffness. This may arise from the fact that, unlike for the quasi-static tests, the strain rate is not constant as the impactor decelerates during compression.

The changes in the stress-strain profiles result in a change in the energy absorption profiles of these structures. Comparisons of the energy absorption profiles of the quasi-static tests and impact tests with $\dot{\epsilon}_{int} = 51\,s^{-1}$ are given in the Supplementary information S2. In all cases there is a shift in the energy absorbing envelope with

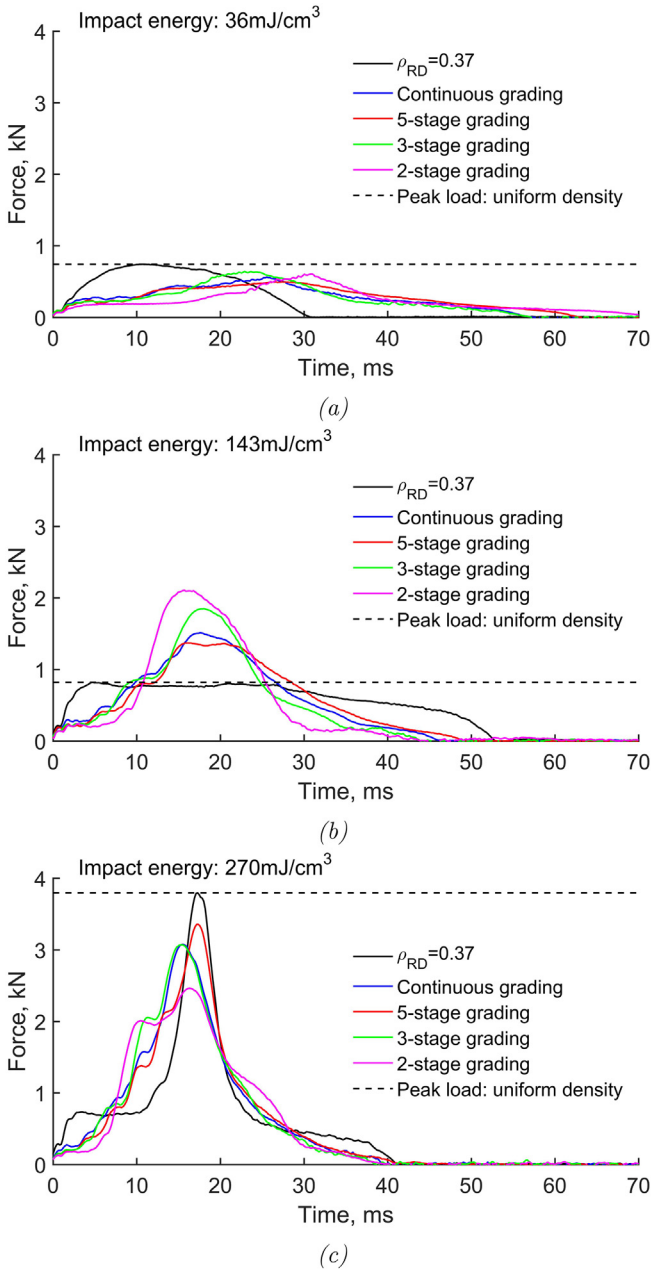

Fig. 8. Force-time plots for graded density honeycombs and uniform density ($\rho_{RD} = 0.37$) reference sample subjected to impacts with specific impact energies of (a) 36 mJ/cm^3, (b) 143 mJ/cm^3 and (c) 270 mJ/cm^3. The peak load transferred by the uniform density structure is indicated by a dashed black line for reference.

increased strain rate such that for $E_S^* > 150$ mJ/cm^3, lower stresses are transferred for higher strain rate impacts. This occurs because the energy required to densify the hexagonal structures is far greater at high strain rates due to material visco-elasticity.

5. Summary and conclusions

This work is the first of its kind to explore the effect of density grading on the energy absorbing and damping behaviour of flexible honeycomb structures. It was seen that by applying density grading to flexible TPU honeycomb structures, the energy absorbing and damping profiles are significantly modified from the uniform density equivalent. It was hypothesised that, by including a range of densities within an individual honeycomb structure, it may be possible to absorb a range of impact energies efficiently. However, for the grading methodologies chosen in this work, gains in energy absorbing efficiency occur only close to densification and at low compression energies. Between these extremes, the uniform density structures outperform the graded structures in terms of energy absorbing efficiency. This being said, due to the higher strain to densification and the non-linear relationship with density and energy absorption, the graded structures absorbed larger amounts of energy than the uniform density equivalent up to densification. This would result in a lower stress being transferred by a graded structure if subject to an extreme impact which causes densification.

Sinusoidal compressive testing showed that the energy dissipation behaviour of all the graded structures increased in a non-linear manner with increase in peak to peak strain ϵ_{pp} from 0.05 to 0.45, compared a the linear increase for the uniform density honeycomb. At $\epsilon_{pp} = 0.45$, where the structures were being compressed to the point just before densification, close to their maximum energy absorbing efficiency, the graded structures dissipated more energy per cycle than the uniform density honeycomb. How this relationship varies with a range of grading methodologies should be further explored as different grading methodologies would result in damping profiles which could be tailored to a specific application. Impact testing revealed that higher strain rates lead to a stiffer response of the honeycombs, as would be expected for a structure formed from a visco-elastic material. As a result, greater total energies were absorbed by the graded structures at high strain rates which should be taken into consideration when designing TPU honeycomb structures for practical energy absorbing applications. The behaviour seen in the quasi-static evaluation, where the graded structures absorbed low and high energy impacts more efficiently than the uniform density structure, was reflected in the results from the impact tests.

Density grading has a clear potential for tailoring the mechanical response of cellular structures. Linear grading was explored in this work but there are limitless grading methodologies which could be explored which include degrees of asymmetry or structural hierarchy. Further, in this work grading was achieved by varying topology, however, energy absorption response could also be manipulated by 3D printing in 2 or more different types of material, which is possible using modern FFF technology. This tailoring method is of interest as it would allow the use of varying stiffness materials in discrete layers to achieve similar behaviour as topological grading. By replacing high density layers with high stiffness layers, part mass could be reduced. The inclusion of materials with different time-varying properties could be used to tailor the mechanical and damping response yet further.

Data availability

The raw/processed data required to reproduce these findings cannot be shared at this time as the data also forms part of an ongoing study.

CRediT authorship contribution statement

Simon R.G. Bates: Conceptualization, Data curation, Formal analysis, Investigation, Methodology, Validation, Visualization, Writing - original draft, Writing - review & editing. **Ian R. Farrow:** Formal analysis, Project administration, Supervision, Writing - review & editing. **Richard S. Trask:** Conceptualization, Funding acquisition, Project administration, Supervision, Writing - review & editing.

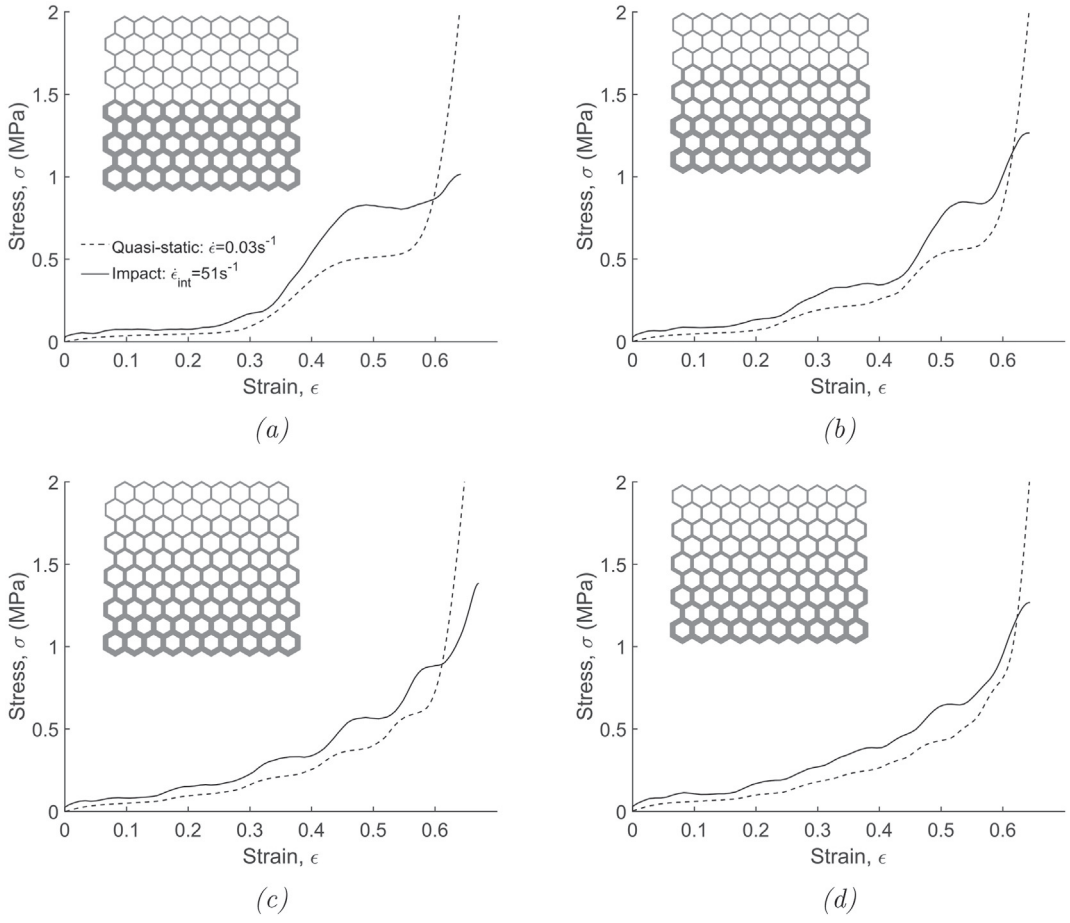

Fig. 9. Stress-strain plots extracted from the compressive behaviour of (a) 2-stage graded, (b) 3-stage graded, (c) 5-stage graded and (d) continuously graded honeycombs under 270 mJ/cm^3 impact. The initial impact strain rate, $\dot{\epsilon}_{int} = 51\,s^{-1}$. The quasi-static ($\dot{\epsilon} = 0.03\,s^{-1}$) stress-strain data for each honeycomb is included for comparison.

Acknowledgments

SRGB has been financially supported by the Engineering and Physical Sciences Research Council (EPSRC) Centre for Doctoral Training in Advanced Composites for Innovation and Science (grant number EP/G036772/1) and the Royal National Lifeboat Institution (RNLI). RST is funded under EPSRC 'Engineering Fellowships for Growth' (grant number EP/M002489/1).

Appendix A. Supplementary data

Supplementary data to this article can be found online at https://doi.org/10.1016/j.matdes.2018.11.019.

References

[1] D. Wang, Z. Wang, Q. Liao, Energy absorption diagrams of paper honeycomb sandwich structures, Packaging Technology and Science 22 (2009) 63–67.
[2] Portigliotti, O. Bayle, L. Lorenzoni, T. Blancquaert, S. Langlois, M. Capuano, T. Walloschek, Exomars entry decent and landing demonstrator mission and design overview, ExoMars EDM Overview Paper, NASA. 2016.
[3] L.J. Gibson, M.F. Ashby, Cellular Solids: Structure and Properties, Second ed., Cambridge University Press, Cambridge, 1999.
[4] T.N. Bitzer, Honeycomb Technology: Materials, Design, Manufacturing, Applications and Testing, Springer - Science and Business Media B.V. 1997.
[5] R. Bagley, Extrusion Method for Forming Thin Walled Honeycomb Structures,uS3790654A. 1974.
[6] Q. Chen, M. Pugno, In-plane elastic buckling of hierarchical honeycomb materials, Eur. J. Mech. A. Solids 34 (2012) 120–129.
[7] R. Oftadeh, B. Haghpanah, D. Vella, A. Boudaoud, A. Vaziri, Optimal fractal-Like hierarchical honeycombs, Phys. Rev. Lett. 113 (104301) (2014).
[8] B. Haghpanah, J. Papadopoulos, D. Mousanezhad, H. Nayeb-Hashemi, A. Vaziri, Buckling of regular, chiral and hierarchical honeycombs under a general macroscopic stress state. Proceedings of the Royal Society A: Mathematical, Phys. Eng. Sci. 470 (2167) (2014) 20130856.
[9] Y. Hou, R. Neville, F. Scarpa, C. Remillat, B. Gu, M. Ruzzene, Graded conventional-auxetic Kirigami sandwich structures: flatwise compression and edgewise loading, Compos. Part B 59 (2014) 33–42.
[10] A. Ajdari, B.H. Jahromi, J. Papadopoulos, H. Nayeb-Hashemi, A. Vaziri, Hierarchical honeycombs with tailorable properties, Int. J. Solids Struct. 49 (2012) 1413–1419.
[11] K. Wang, Y.H. Chang, Y. Chen, C. Zhang, B. Wang, Designable dual-material auxetic metamaterials using three-dimensional printing, Mater. Des. 67 (2015) 159–164.
[12] D. Mousanezhad, R. Ghosh, A. Ajdari, A.M.S. Hamouda, H. Nayeb-Hashemi, A. Vaziri, Impact resistance and energy absorption of regular and functionally graded hexagonal honeycombs with cell wall material strain hardening, Int. J. Mech. Sci. 89 (2014) 413–422.
[13] S. Limmahakhun, A. Oloyede, K. Sitthiseripratip, Y. Xiao, C. Yan, Stiffness and strength tailoring of cobalt chromium graded cellular structures for stress-shielding reduction, Mater. Des. 114 (2017) 633–641.
[14] S. Ying, C. Sun, K. Fai, J. Wei, Compressive properties of functionally graded lattice structures manufactured by selective laser melting, Mater. Des. 131 (2017) 112–120.
[15] A. Ajdari, H. Nayeb-Hashemi, A. Vaziri, Dynamic crushing and energy absorption of regular, irregular and functionally graded cellular structures, Int. J. Solids Struct. 48 (3–4) (2011) 506–516.
[16] L. Cui, S. Kiernan, M.D. Gilchrist, Designing the energy absorption capacity of functionally graded foam materials, Mater. Sci. Eng. A 507 (2009) 215–225.
[17] N. Gupta, A functionally graded syntactic foam material for high energy absorption under compression, Mater. Lett. 61 (2007) 979–982.
[18] Y. Hangai, K. Takahashi, T. Utsunomiya, K. Soichiro, O. Kuwazuru, N. Yoshikawa, Fabrication of functionally graded aluminum foam using aluminum alloy die castings by friction stir processing, Mater. Sci. Eng. A 534 (2012) 716–719.

[19] A.H. Brothers, D.C. Dunand, Mechanical properties of a density-graded replicated aluminum foam, Mater. Sci. Eng. A 489 (2008) 439–443.
[20] I. Maskery, A. Hussey, A. Panesar, A. Aremu, C. Tuck, I. Ashcroft, R. Hague, An investigation into reinforced and functionally graded lattice structures, J. Cell. Plast. 0 (0) (2016) 1–15.
[21] X-c. Zang, L.-q. An, H.-m. Ding, Dynamic crushing behavior and energy absorption of honeycombs with density gradient, J. Sandw. Struct. Mater. 16 (2014) 125–147.
[22] P. Zhang, D.J. Arceneaux, A. Khattab, Mechanical properties of 3D, printed polycaprolactone honeycomb structure, J. Appl. Polymer Sci. 135 (2017) 46018.
[23] J. Yi, M.C. Boyce, G.F. Lee, E. Balizer, Large deformation rate-dependent stress-strain behavior of polyurea and polyurethanes, Polymer 47 (1) (2006) 319–329.
[24] C. Ge, L. Priyadarshini, D. Cormier, L. Pan, J. Tuber, A preliminary study of cushion properties of a 3D printed thermoplastic polyurethane Kelvin foam, Packag. Technol. Sci. 31 (2018) 361–368.
[25] S. Bates, I. Farrow, R. Trask, 3D printed polyurethane honeycombs for repeated tailored energy absorption, J. Mater. Des. 112 (2016) 172–183.
[26] A.S.T.M. Standards, Standard Test Methods for Vulcanized Rubber and Thermoplastic Elastomers Tension,D412-06A. ASTM International, West Conshohoken PA, 2006.
[27] K. Wang, Y.H. Chang, Y. Chen, C. Zhang, B. Wang, Designable dual-material auxetic metamaterials using three-dimensional printing, Mater. Des. 67 (2015) 159–164.
[28] Ultimaker Original General Specifications, Available at: https://Ultimaker.Com/En/Products/Ultimaker-Original/Specifications, Accessed date: 10 July 2018.
[29] Flex3drive Filament Driver for Ultimaker Original, Fex3drive, https://Flex3drive.Com/Flex3drive/F3d-Umo, Accessed date: 10 July 2018.
[30] Repetier-Host software, Available at: https://www.repetier.com/, Accessed date: 10 July 2018.
[31] Cura by Ultimaker Slicing Software, Available at: https://Ultimaker.Com/En/Products/Cura-Software, Accessed date: 10 July 2018.
[32] M. Avalle, G. Belingardi, Montanini Characterization of polymeric structural foams under compressive impact loading by means of energy-absorption diagram, Int. J. Impact Eng. 25 (2001) 455–472.
[33] H.J. Qi, M.C. Boyce, Stress-Strain Behavior of Thermoplastic Polyurethane, Dissertation. Massachusetts Institute of Technology. 2004.
[34] L. Dong, R.S. Lakes, Advanced damper with negative structural stiffness elements, Smart Mater. Struct. 21 (2012) 1–17.
[35] Z. Zou, S.R. Reid, P.J. Tan, S. Li, J.J. Harrigan, Dynamic crushing of honeycombs and features of shock fronts, International Journal of Impact Engineering 36 (1) (2009) 165–176.